Plasmon enhanced light scattering into semiconductors by aperiodic metal nanowire arrays

Ulriksen, Hans Ulrik; Søndergaard, Thomas Møller; Pedersen, Thomas Garm; Pedersen, Kjeld

Published in:
Optics Express

DOI (link to publication from Publisher):
10.1364/OE.27.014308

Publication date:
2019

Document Version
Publisher's PDF, also known as Version of record

Research Article | Vol. 27, No. 10 | 13 May 2019 | OPTICS EXPRESS 14308
Optics EXPRESS

Plasmon enhanced light scattering into semiconductors by aperiodic metal nanowire arrays

H. U. ULRIKSEN,* T. SØNDERGAARD, T. G. PEDERSEN, AND K. PEDERSEN

Department of Materials and Production, Aalborg university, Skjernvej 4, 9220 Aalborg East, Denmark
*huu@nano.aau.dk

Abstract: Light scattering from nanostructures is an essential ingredient in several optical technologies, and experimental verification of simulations of light scattering is important. In particular, solar cells may benefit from light-trapping due to scattering. However, light that is successfully trapped in an absorbing media such as e.g. Si necessarily escapes direct detection. We present in this paper a technique for direct measurement and analysis of light scattering from nanostructures on a surface, exemplified with aperiodic patterns of Ag strips placed on a GaAs substrate. By placing the structures on the flat face of a half-cylinder, the angular distribution of light scattered into the azimuth plane can be directly detected, including directions above the critical angle that would be captured if the substrate had the form of a slab. Modelling of the scattered light by summing up contributions from each strip agrees with the experimental results to a very detailed level, both for scattering backward and into the substrate.

1. Introduction

Metallic nanoparticles have been intensively studied due to the strong scattering at the particle plasmon frequency [1–3]. A special case is nanostructures on a surface which is of interest for applications such as optical nanoantennas [4] and light-trapping in thin-film solar cells [1,2]. High-refractive-index substrates are of particular interest since they have a large effect on the scattering properties. These applications rely not only on the strong scattering of nanostructures but also the ability to control the direction of the scattered light. The scattering and absorption cross-sections of plasmonic metal nanoparticles have previously been studied both theoretically [5–8] and experimentally [5, 9, 10], and the mechanisms governing these properties are well understood. For thin-film solar cells in particular, the angular distribution of light scattered on a nanostructure is important in order to trap as much light as possible. Hence, it is sought to maximize the fraction scattered into the substrate and to scatter the light into angles above the critical angle. The theoretical work in this area is extensive and covers a range of sample geometries, such as a scatterer above or on a surface [8, 11–13] and a scatterer in a sandwich structure [6, 14]. Experiments measuring the angular distribution of light have primarily focused on emission from a single scatterer using dark-field microscopy [15, 16] or special mirrors [17]. Other experiments measure the angular distribution of light scattered off an ensemble of nanoparticles [18], but here the single-particle angular distribution is lost and it is typically light scattered into air which is measured.

For analysis and optimization purposes it is important to verify the simulated properties of nanostructures. Such verification can be difficult, however, in the actual device geometry due to light-trapping and absorption. For instance, the absorption in silicon (Si) is sufficiently high to make it difficult to detect light scattered into the Si substrate, in particular with wavelengths of interest for solar cell applications, and to obtain sufficient signal-to-noise ratio, while maintaining the angular information. Hence, in this paper we present a practical and simple method to address

#360739 https://doi.org/10.1364/OE.27.014308
Journal © 2019 Received 21 Feb 2019; revised 9 Apr 2019; accepted 11 Apr 2019; published 2 May 2019

Optics EXPRESS

these issues. A simple experiment is constructed where the angular spectrum of light scattered into the semiconductor can be determined directly using an angle scanning setup [19]. This is achieved by placing the structures on the flat side of a half-cylinder, near the center axis of the cylinder. The scattering angles into the cylinder material can be determined by detecting the angular spectrum transmitted through the cylindrical surface. As Gallium arsenide (GaAs) has almost the same refractive index as Si just below the Si bandgap, but very low absorption, the experiments are performed using a GaAs half-cylinder and a laser diode with a wavelength of 980 nm. This allows us to directly observe the scattering angles as well as the scattering cross-section of the structures. Hence, we demonstrate that the proposed method is a useful and accurate tool for verification of simulated angular scattering profiles of relevance for e.g. plasmon-enhanced solar cells.

2. Theory

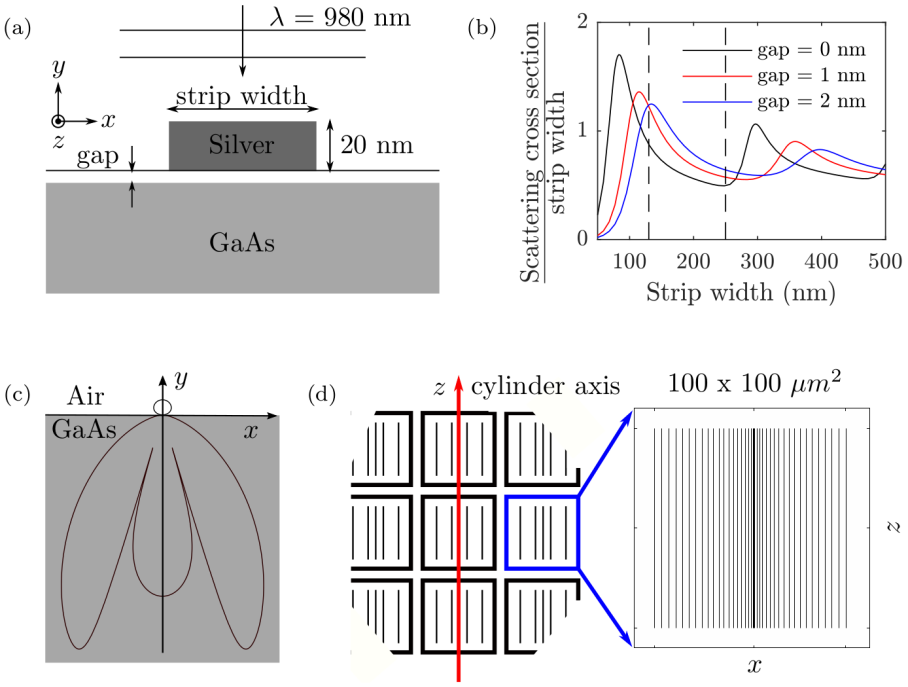

Fig. 1. (a) Sample geometries for a single strip. (b) Scattering cross section as a function of strip width for 3 different gap sizes. The dashed lines represent the strip width on the two samples that have been fabricated. (c) Scattering per unit angle into both air and substrate for a 130 nm strip. (d) Schematic illustration of the structure written on the flat side of the half-cylinder.

2.1. A single strip

The scattering of light by a large number of Ag nanostrips on a GaAs surface will, in this paper, be modelled by superposing scattered fields originating from each nanostrip. At normal incidence and in-plane polarization perpendicular to the strips there is very little scattering in the x-direction (see Fig. 1(a)), except for the generated near-field. The combination of a thick substrate, a relatively large distance between strips, and the aperiodic structure, allows us to neglegt multiple scattering between nanostrips, inter-strip coupling [20, 21] and surface-modes.

Received 21 Feb 2019; revised 9 Apr 2019; accepted 11 Apr 2019; published 2 May 2019

Optics EXPRESS

The total scattered field is thus obtained as the scattered field from a single nanostrip multiplied by a factor that takes into account the different propagation distances from each nanostrip before the light reaches the detector.

The scattering by a single Ag nanostrip on a GaAs surface being illuminated by a normally incident plane wave (see Fig. 1(a)) has been calculated by using the Green′s function surface integral equation method (GFSIEM) [22] for 2D scattering problems. The nanostrip is assumed to be of infinite length (along the z-axis), and the electric field is polarized along the x-axis. The corners of the nanostrip are rounded with a 2-nm corner radius. The thickness of the nanostrip is 20 nm, and the wavelength is 980 nm. According to the literature [23, 24] a native oxide layer on the GaAs is estimated to be from 0.5 nm to app. 2 nm depending on oxidation time. We take into account the effect of this layer by adding a small air-gap between the strip and the GaAs surface. The scattering cross section, i.e., the total scattered power normalized to the incident power per unit area, is shown in Fig. 1(b) as a function of strip width. By normalizing the scattering cross section with the strip width resonances can be easily identified. The resonances are due to the excitation of surface plasmon polaritons propagating back and forth across the Ag strips (along x) and being reflected at the strip edges. This leads to standing-wave resonances when the total round-trip propagation and reflection phase is an integer multiple of 2π. The peaks in Fig. 1(b) are due to excitation of the 1st and 3rd order standing-wave resonances. The 2nd order resonance cannot be excited when using normally incident light due to symmetry considerations [22]. By assuming an oxide layer thickness of 1-2 nm a peak is found at the strip width of app. 130 nm, while a strip width of 250 nm being also considered in the paper is mid between resonances. The scattered radiation pattern (or differential scattering cross section) for a 130-nm-wide strip is shown in Fig. 1(c). Most of the scattered light goes into the semiconductor substrate, which is a consequence of the large refractive index of GaAs compared with air [22]. In addition, a large fraction of the scattered light is at angles that are above the critical angle of a GaAs-air interface ($\approx 17^\circ$ at 980 nm). A plane wave being incident on a planar GaAs-air interface, i.e., from the GaAs side at an angle above the critical angle, would be totally internally reflected. In the case of a GaAs film this means that the light would be trapped in the GaAs, which is useful for a solar cell. The radiation pattern is almost the same as the one for a 30-nm-wide and 17-nm thick strip (see [22]), which is because in both cases the strip width is significantly smaller than the wavelength, and the radiation pattern is similar to that of a dipole in both cases.

2.2. Array of strips – reflection

To obtain a large signal-to-noise ratio of the measured scattered light, one strip is not enough. Introducing more strips with equidistant spacing gives rise to sharp diffraction peaks, which, in connection with the experiment, is undesirable as all information of the scattering profile for a single strip is lost. To circumvent this we place the Ag strips in an aperiodic array to diffract the light into a broad range of angles and thereby obtain information on the scattering profile. To model the measured radiation pattern from the multiple strips we divide the model into two cases: backscattered light and light scattered into the substrate. In each case we assume the structures to be invariant along the z-axis.

For the backscattered case the model is straight forward. The detector is moved around the half-cylinder at angles up to $\theta = 90^\circ$ as illustrated in Fig. 2(a). At large distances from the strip the scattered field will propagate roughly as a cylindrical wave and for each detector angle (θ), see Fig. 2(b), the electric field at detector angle θ is calculated as

$$E(\theta) = F \sum_p \frac{S(\alpha_p) \exp(-ik_0 r_p) \exp\left(\frac{-(x_p - x_c)^2}{w^2}\right)}{r_p}. \quad (1)$$

Here, F is a scaling factor, $S(\alpha_p)$ is the square root of the single-strip radiation pattern (Fig. 1(c))

Received 21 Feb 2019; revised 9 Apr 2019; accepted 11 Apr 2019; published 2 May 2019

Optics EXPRESS

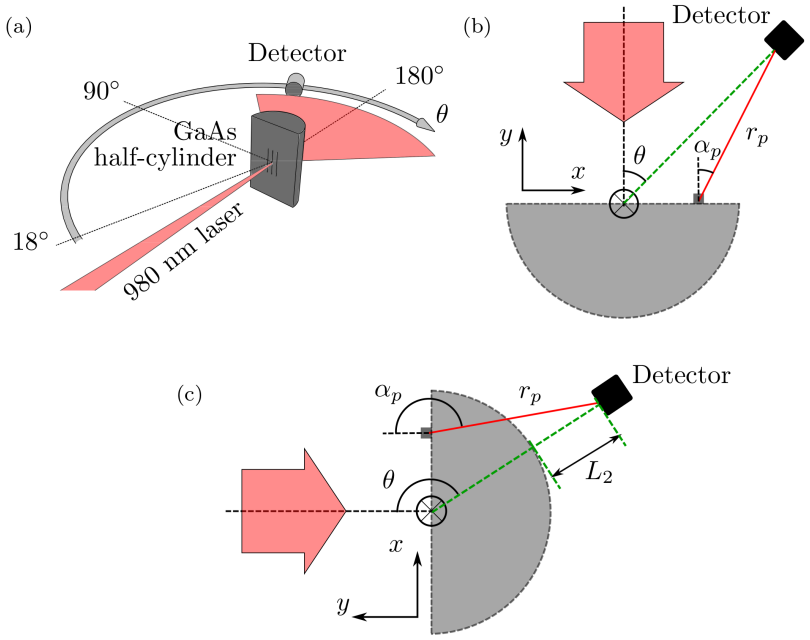

Fig. 2. (a) Detector setup. (b) Sketch showing angles and distances used in the model for reflection. (c) Sketch showing angles and distances used in the simple model for transmission.

at angle α_p (see Fig. 2(b)), k_0 is the free-space wave-number, and r_p is the distance from strip number p to the detector, also, x_p is the strip position on the surface for strip p, x_c is the position of the center axis of the incident beam relative to the center of the write-field, and w is the width of the incident Gaussian beam on the surface.

2.3. *Array of strips – transmission*

For light scattered into the substrate the problem is more complex for two reasons mainly. First, the distance traveled by light from the individual strip to the detector varies a great deal due to refraction and the curved backside. Second, the scattering intensity depends highly on the angle, as seen in Fig. 1(c).

One could question the need to include the effects mentioned above for the forward scattering and attempt a simpler approach much like Eq. (1). In such a simple model we assume that light from each strip also travels to the sensor in a straight line, neglecting the curved backside and the refraction of light as illustrated in Fig. 2(c). Again, the detector rotates around the fixed axis, now at angles above $\theta = 90°$. The distance from strip to sensor, r_p, is easily calculated, and if L_2 (see Fig. 2(c)) is assumed the same for every strip, the distance travelled in GaAs follows directly. The electric field at the detector angle θ is then calculated as

$$E(\theta) = TF \sum_p \frac{S(\alpha_p)\exp(-ik_0 n_1 L_{1,p})\exp(-ik_0 L_2)\exp\left(\frac{-(x_p-x_c)^2}{w^2}\right)}{r_p}. \quad (2)$$

T is the transmission coefficient of the GaAs to air interface, n_1 is the complex refractive index of GaAs, and $L_{1,p} = r_p - L_2$ is the distance traveled in GaAs. As will be apparent in Sec. 4.4 this model does not describe the measured signal and the effect of the curved backside must be considered.

Received 21 Feb 2019; revised 9 Apr 2019; accepted 11 Apr 2019; published 2 May 2019

Optics EXPRESS

The issues arising from the curved backside are illustrated in Fig. 3. If a strip is placed at the center of rotation, the distance travelled in the substrate is the same as the half-cylinder radius (R), the distance travelled in air is $L_2 = L - R$, and the detector angle θ is the same as the angle of the scattered light detected. For strips placed off center all three are changed into θ', L_1' and L_2'. Due to the relatively small radius of the cylinder and the high refractive index of GaAs, all three effects are significant and cannot be neglected.

To correct for these effects we introduce the two parameters δ and α', both illustrated in Fig. 3. δ is the change in the optical path length in air and α' is the change in angle, relative to the detector angle, of the scattered light reaching the detector. Moreover, we found it necessary to introduce a fitting-parameter (y' in Fig. 3) to account for a mismatch in rotational axis and surface. The angles in Fig. 3 are greatly exaggerated and are in the experiment very small, thus,

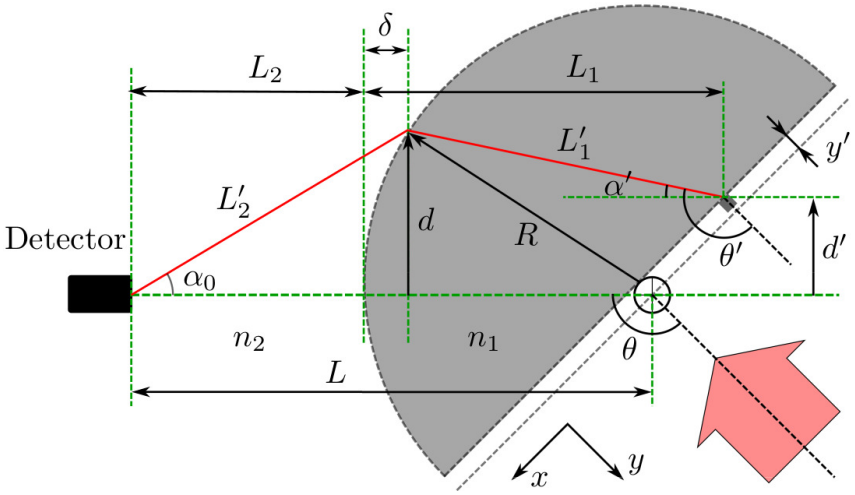

Fig. 3. Sketch of sample and detector system. The sketch is not to scale, L = 0.30 m and R = 2.7 mm.

both δ and α' can be estimated via the matrix method in paraxial optics;

$$\begin{bmatrix} d_0 \\ \alpha_0 \end{bmatrix} = \begin{bmatrix} 1 & L_2 \\ 0 & 1 \end{bmatrix} \begin{bmatrix} 1 & 0 \\ \frac{n_1 - n_2}{R n_2} & \frac{n_1}{n_2} \end{bmatrix} \begin{bmatrix} 1 & L_1 \\ 0 & 1 \end{bmatrix} \begin{bmatrix} d' \\ \alpha' \end{bmatrix}. \tag{3}$$

We define the optical axis as the straight line between the rotational axis and the detector. d_0 is the height above the optical axis of the light-beam at the detector and is always zero as the detector per definition is on the optical axis. α_0 is the angle of the light-beam at the detector. d' is the strip height above the optical axis and can for each strip be calculated as $d' = y'\cos(\theta) + x'\sin(\theta)$, where x' is the position of the strip on the surface, and y' is the surface offset (see Fig. 3). We calculate $L_1 = R - y'\sin(\theta) + x'\cos(\theta)$ and $L_2 = L - R$, where L is the distance from center of rotation to the detector and R is the radius of the half-cylinder. n_1 and $n_2 = 1$ are the refractive indices of the substrate and air, respectively. By solving Eq. (3) one obtains both α_0 and α'. To calculate δ we estimate $d = L_2\tan(\alpha_0)$ and then $\delta = R - \sqrt{R^2 - d^2}$. The corrected distance for each strip in both substrate and air is then

$$\begin{aligned} L_1' &= (L_1 - \delta)/\cos(\alpha') \\ L_2' &= (L_2 + \delta)/\cos(\alpha_0). \end{aligned} \tag{4}$$

Finally, the laser beam has a Gaussian beam profile with a width w, thus each strip is not illuminated equally. We end up with an expression for the total electric field at each detector

Received 21 Feb 2019; revised 9 Apr 2019; accepted 11 Apr 2019; published 2 May 2019

Optics EXPRESS

position as

$$E(\theta) = TF \sum_p \frac{S(\theta'_p) \exp(-ik_0 n_1 L'_{1,p}) \exp(-ik_0 L'_{2,p}) \exp\left(\frac{-(x'_p - x_c)^2}{w^2}\right)}{L'_{1,p} + L'_{2,p}}. \quad (5)$$

T is the transmission coefficient of the GaAs to air interface, F is a scaling factor, $S(\theta'_p)$ is the square root of the scattering intensity per unit angle in direction $\theta'_p = \theta + \alpha'_p$. x'_p is the strip position on the surface for strip p. Finally a simple moving average is applied to model the width of the detector.

The sample is mounted on a 5-axis stage when the structures are written using e-beam lithography. This gives an uncertainty on the positions of the write-fields relative to each other. This write-field stitching error must be accounted for in the model, but will result in a large number of variables if the position of all illuminated write-fields should be free to move. In order to limit the number of free variables in the models, we assume z invariance and that only three write-fields are illuminated. This is reasonable as the full width half maximum (FWHM) of the laser beam is 160 μm. This limits the free variables of the back scatter model to two write-field stitching, one beam-center and a scaling factor. For the forward scatter model we reuse the former values and need only one free parameter, the GaAs surface offset. The GaAs half-cylinder was grinded and polished by hand and imperfections in the shape of the half-cylinder are expected. As a consequence, prior to the experiment, a calibration of the half-cylinder was performed by a number of different diffraction gratings written on the half-cylinder. The gratings were made using e-beam lithography. The measured diffraction angles for each grating were then compared to the theoretical value to make a calibration curve. As a final remark, this method is not limited to any particular ordering of the strips or specific polarization of light. However, the array must be aperiodic with sufficient gap between strips. Within this limitation the proposed method can be applied to general scattering geometries and any polarization of the incidence light.

2.4. Summary of model

The list below gives an overview of how the different parameters for the models are obtained.

General assumptions:

Three write-fields, z invariance and cylindrical waves.

Measured quantities:

Width of the beam, distance from the cylinder axis to the detector, radius of the half-cylinder, calibration of the half-cylinder.

Model of the backscattered light

Free parameters: Write-field stitching error, beam-center position and scaling factor.

Model of the forward scattered light

From backscattering model: Write-field stitching error, beam-center position and scaling factor.

From literature: Refractive index of substrate.

Free parameters: The GaAs surface offset.

Received 21 Feb 2019; revised 9 Apr 2019; accepted 11 Apr 2019; published 2 May 2019

Optics EXPRESS

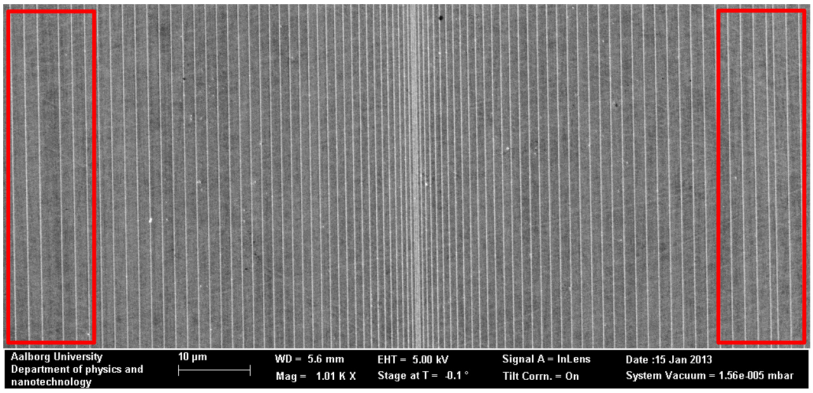

Fig. 4. SEM image showing the full width of a 100 x 100 μm^2 write-field with 130 nm Ag strips. Write-field stitching errors are seen in the red squares.

3. Experimental

The experimental setup is shown in Fig. 2(a). Laser light with a wavelength of 980 nm from a continuous laser-diode is focused with a 200 mm focal length lens onto the flat side of the half cylinder at normal incidence. The FWHM of the beam at focus has been measured to 160 μm. We use a Si detector mounted on an arm with a length of L = 0.30 m that can be rotated around the half-cylinder and all intensities are obtained from a single measurement. The half cylinder used in the experiment has a radius of R = 2.7 mm and is made of crystalline GaAs. The Ag strips are made by a standard e-beam lithography and lift-off procedure and are placed near the center on the flat side of the half-cylinder, with all strips parallel to the cylinder axis.

Specifically, two different samples have been fabricated, one with strips of 130 nm width and one with 250 nm width, all with a thickness of 20 nm. The width of 130 nm is chosen as it is expected to be at a plasmon resonance, whereas 250 nm is between two resonances, and a weak plasmon effect is expected, see Fig. 1(b). The e-beam-setup has a writing area of 100 x 100 μm^2, so both the 130 nm area and the 250 nm area are made of several identical write-fields written close together (see Fig. 1(d)).

The strips must be placed in an aperiodic manner and the exact position of each strip must be known. This is possible using e-beam lithography and for this experiment we have chosen the following position for each strip on a write-field of 100 x 100 μm^2

$$x_p = \pm 50\mu m \left(\frac{p}{p_{max}}\right)^{1.4}, p = 1, 2, 3, \ldots, p_{max} \tag{6}$$

where x_p is the position of strip p and p_{max} is the number of strips in one half of the write-field. The number of strips is determined by the required coverage

Both the 130 nm area and 250 nm area are designed to have a strip coverage of 10%, which leads to 77 strips and 40 strips on a 100 x 100 μm^2 area, respectively. For the 130 nm sample the range of periods spans from 0.24 μm to 1.83 μm . A SEM image of a part of a 100 x 100 μm^2 write-field with 130 nm strips is shown in Fig. 4. Also indicated in the red squares on Fig. 4 are write-field stitching errors, which can lead to both an increase and a decrease in the distance between the outer strips of two neighboring write-fields.

Received 21 Feb 2019; revised 9 Apr 2019; accepted 11 Apr 2019; published 2 May 2019

Optics EXPRESS

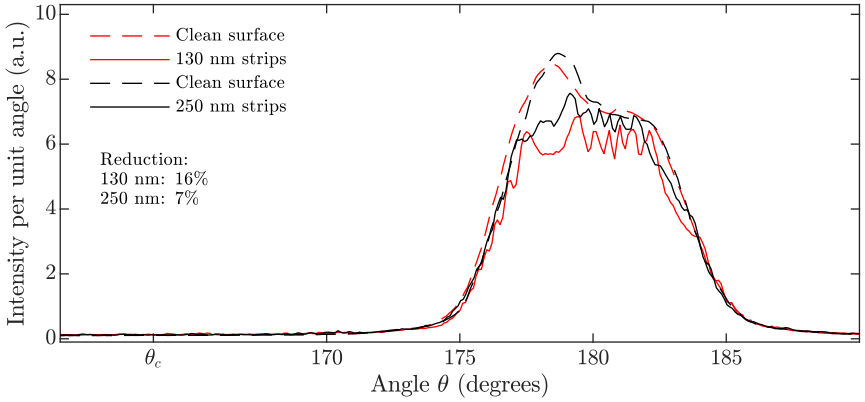

Fig. 5. Measured intensity of the transmitted light for the setup illustrated in Fig. 2(a). The incidence light is polarized transverse to the strips and results are shown for the aperiodic array of 130 nm and 250 nm Ag strips and the same areas without strips.

4. Results

4.1. Direct transmission

The level of interaction between light and nanostructures, both in terms of scattering and absorption, is an important property to investigate. Figure 5 shows the intensity of the directly transmitted beam. The polarization of the incidence light is transverse to the strips and results are shown both for the 130 nm and the 250 nm strips and for the same areas with no strips. The asymmetry in the directly transmitted beam, especially for the clean surface, is related to the beam quality of the laser diode used in the experiment. The reductions indicated in Fig. 5 represent the difference in directly transmitted light, with and without strips. It is calculated by comparing the integrated intensity per unit angle between the critical angles (from 163° to 197°) for the same area, with and without strips. Thus, the reductions represent the light that is lost via absorption, reflection and scattering into angles larger than the critical angle due to the Ag strips. For the 130 nm wide strips (see Fig. 5) we see a larger decrease in transmitted light compared to the case of 250 nm strips, i.e, $\approx$ 16% and $\approx$ 7%. This corresponds well with the expected resonance for the 130 nm strip (see Fig. 1(b)). The difference in magnitude of scattering out of the direct beam is also evident in Fig. 1(b), where the cross section per strip width on resonance is twice as large as off resonance. This comparison is posible as both areas have a 10 % strip coverage. The measured reduction contains both reflection, absorption and scattering, but at this structure size, scattering is the dominating effect [6, 9].

4.2. Scattered light – reproducibility

We now turn our attention to the diffracted light, starting with the total scattered light and means of tracking changes in the properties of nanostructures. Figure 6 shows the intensity of the light scattered off the aperiodic array of 130 nm Ag strips on the GaAs surface and is defined as $I_s = I - I_0$ where I is the measured intensity with strips and I_0 is the measured intensity without strips. The black line is the intensity from a new sample, whereas the red line is the intensity from the same sample, but 80 days older. The scattered intensity for the 80 days old sample has been multiplied by a factor of 8. Angles from 0° to 90° are backscattered light and from 90° to 180° is light scattered into the substrate and transmitted through the half-cylinder. The 90° to 180° intensity has been corrected for transmission and reflection losses. The green line is the calculated scattering per unit angle for a single strip and is equivalent to the one shown in Fig. 1(c). First, the ratio of backward to forward scattered light can be directly assessed and

Received 21 Feb 2019; revised 9 Apr 2019; accepted 11 Apr 2019; published 2 May 2019

Optics EXPRESS

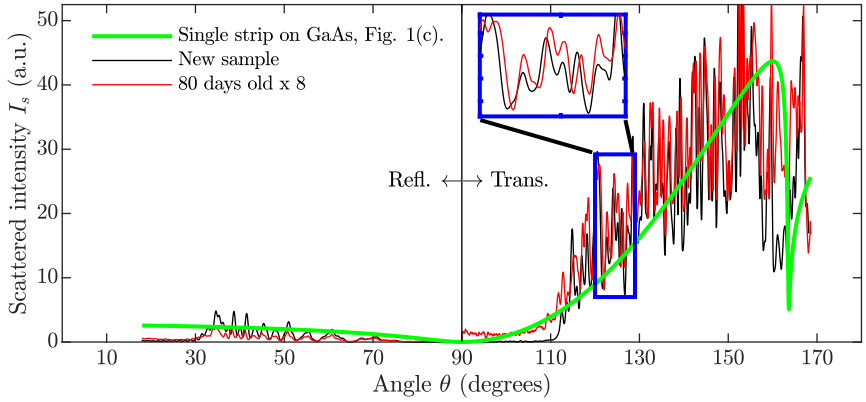

Fig. 6. Measured scattered intensity of the diffracted light from the aperiodic array of 130 nm Ag strips. The green line shows scattering per unit angle for a single 130 nm Ag strip on a GaAs surface. The black line is the measured signal for a new sample, while the red line is for an 80 days old sample multiplied by a factor of 8. The transmitted intensity has been corrected for transmission and reflection losses.

compared with the calculated profile(see Fig. 1(c)). Second, we see that our measurements for the new and 80-day old sample show the same complex peak pattern and intensity distribution except for a scaling factor where the intensity is much lower for the old sample. Exposure to the atmosphere is known to affect Ag nanostructures and both reduce plasmon effects and shift resonances [25, 26] which, in this case, results in a large decrease in scattering cross-section and thereby the scattered intensity. The interference between light scattered from the individual strips is clearly visible as a large number of peaks forming a complex pattern. As illustrated, this pattern is largely unaffected by the oxide layer, and the position of the peaks is reproducible. Thus this method is a strong tool for tracking changes in the properties of the nanostructures.

4.3. *Backscattered light*

We now discuss the details of the diffraction pattern. First, we consider the backscattered light. The red line in Fig. 7(a) shows the measured intensity of the backscattered light from the aperiodic array of 130 nm Ag strips. The black line in Fig. 7(a) is the calculated backscattered light using Eq. (1) and the green line shows the scattering per unit angle from a single 130 nm Ag strip on a GaAs surface. We have restricted ourself to three write-fields in the model, which are perfectly placed next to each other with no write-field stitching error (Fig. 4). The strips are infinitely long and the beam is perfectly centered on the middle write-field. Both the measured signal and the calculated spectra (F in Eq. (1)) have been scaled to a maximum intensity of one. With these initial parameters our model shows some resemblance with the measured signal. Both the strong onset of signal around 30 degree, which is caused by diffraction from the long period part (1.83 μm) of the aperiodic array, and large scale features at high angle are modeled with some success.

To improve our model we include the write-field stitching error and the position of the beam center axis by allowing the two outer fields and the beam (x_c) to move, still using Eq. (1). Optimizing the position of the write-fields and the beam in the model resulted in the calculated graphs in Fig. 7(b), again, both the measured signal and the calculated spectra have been scaled to a maximum intensity of one. We obtained the best result with the following movements: left write-field shift 0, right write-field shift 0.9 μm, and x_c = 7 μm. The write-field shifts are within the accuracy of 1-2 μm for the stage in the e-beam lithography setup. The center of the half-cylinder surface can be found with comparable precision, and a x_c value of 7 μm is

Received 21 Feb 2019; revised 9 Apr 2019; accepted 11 Apr 2019; published 2 May 2019

Optics EXPRESS

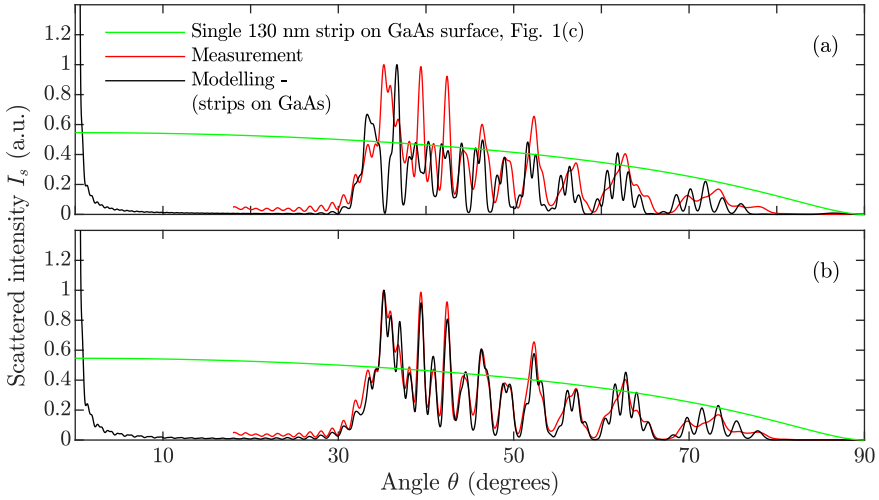

Fig. 7. In both (a) and (b), the green lines shows the scattering per unit angle from a single 130 nm Ag strip on a GaAs surface. The red line is the measured signal from the aperiodic array of 130 nm Ag strip and the black lines are the calculated signals using Eq. (1). In (b) the positions of the write-fields and the beam center have been optimized to match modelling and measurements.

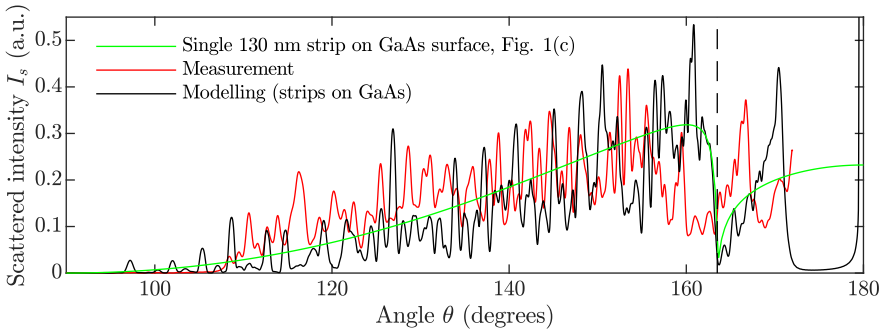

Fig. 8. The green line shows the scattering per unit angle from a single130 nm Ag strip on a GaAs surface. The red line is the measured signal from the aperiodic array of 130 nm Ag strips and the black line is the calculated signal using Eq. (2). The model is corrected for transmission and reflection losses. In the model we have used the write-field stitching error, beam axis position and scaling factor obtained from the modelling of the backscattered light. The dashed vertical line at $\approx 163^\circ$ represents the critical angle for the GaAs-air interface.

within the expected range when also considering imperfections in the shape of the half-cylinder. This has a large impact on the model for the backscattered light, which is now very close to the measured signal. Both the peak positions and the intensity of each peak fit well with the measured ones. The small differences probably originate from the fact that we only use three write-fields and neglect write-fields above and below these three which also contribute to the signal.

4.4. *Forward scattering*

First, we compare the result of modelling using Eq. (2) with the measured signal for the aperiodic array of 130 nm Ag strips. The result is presented in Fig. 8, where the black line is the model, the red line is the measured signal and the green line is the scattering per unit angle for the

Received 21 Feb 2019; revised 9 Apr 2019; accepted 11 Apr 2019; published 2 May 2019

Optics EXPRESS

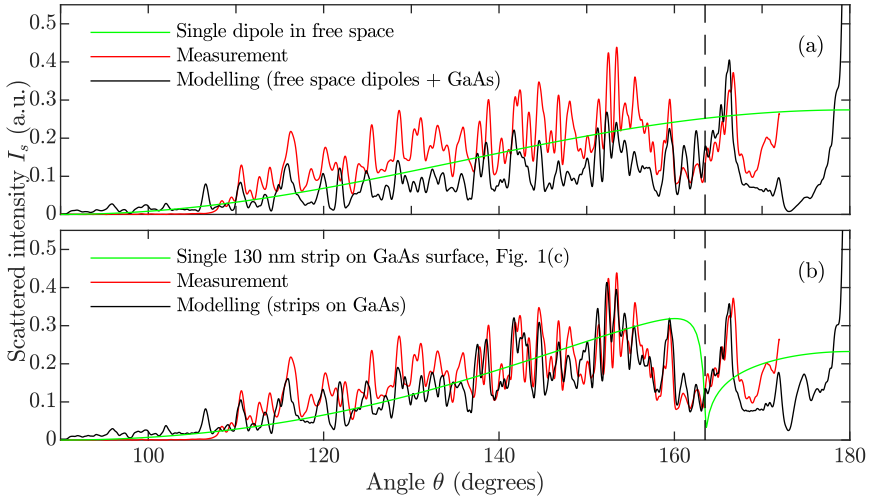

Fig. 9. In both (a) and (b), the green lines shows the scattering per unit angle from a single strip on which the respective models in (a) and (b) are based. The red line is the measured signal from the the aperiodic array of 130 nm Ag strips and the black lines are the calculated signals using Eq. (5) based on (a) free space dipole scattering and (b) the radiation pattern from a 130 nm wide Ag strip on a GaAs surface (see Fig. 1(c)). The models are corrected for transmission and reflection losses. In both models we have used the write-field stitching error, beam axis position and scaling factor obtained from the modelling of the backscattered light. The dashed vertical line at $\approx 163^\circ$ represents the critical angle for the GaAs-air interface.

single 130 nm Ag strip on GaAs. The critical angle for a GaAs-air interface is represented by the vertical dashed line. The model is corrected for transmission and reflection losses and, finally, we have used the write-field stitching error, beam axis position and scaling factor obtained from the backscattering model. The modelling is based on a GaAs refractive index of $n = 3.52 + i0.000083$ at a wavelength of 980 nm, as obtained from interpolating Sopra SA data [27]. The result clearly shows the need for a more detailed model for the forward scattered light. Despite the information obtained from the backscattering, the simple model only agrees on the overall intensity of the forward scattered light.

In Fig. 9 the results using the detailed model (Eq. (5)) are presented. The figure contains two separate graphs, each with the measured signal from the aperiodic array of 130 nm Ag strips in red, the modelling in black, the scattering per unit angle for a single 130 nm Ag strip in green and a vertical black line representing the critical angle. In Figs. 9(a) and 9(b) the models are the same but are based in 9(a) on $S(\alpha_p)$ for a dipole in free space and in 9(b) on $S(\alpha_p)$ for the 130 nm Ag strip on a GaAs surface (Fig. 1(c)). Like the previous simple model, the calculations are corrected for transmission and reflection losses. The results have been obtain using the write-field stitching error, beam axis position and scaling factor obtained from the backscattering model, and by optimizing the surface offset (y'). We obtained the best result with a surface offset of $y' = 210\ \mu$m, which is reasonable considering the experimental setup where the rotational axis of the detector and the center axis of the half-cylinder are aligned using the sample-stage with no direct indication of overlap. The results are very convincing when using the radiation pattern in Fig. 1(c), with good agreement between theory and experiment. For the model using free-space dipole scattering, the peak pattern is equally well described, but some deviations with respect to the intensity level appear. The peak pattern is fixed by the strips positions on the substrate whereas the intensity is related to both the strips position and the scattering per unit angle used in

Received 21 Feb 2019; revised 9 Apr 2019; accepted 11 Apr 2019; published 2 May 2019

Optics EXPRESS

the model.

5. Conclusion

A technique has been presented for verification of simulated light-scattering from surface nanostructures, with particular focus on verification of the angular scattering profile of a single scatterer. The technique is based on using multiple scatterers placed in an aperiodic array for increasing the signal-to-noise ratio, and at the same time maintaining angular information of the light-scattering from a single scatterer. By placing the scatterers on the flat face of a half-cylinder, the light scattered into the surface is coupled out through the curved sides of the cylinder, such that the angular profile of light scattered into the substrate can be measured. A thick substrate in combination with the aperiodic array allows us to treat the scatterers as non-interacting, provided we use a sufficiently large distance between neighboring scatterers. This leads to a detailed model for scattering from the aperiodic array based on summing up contributions from each scatterer using the scattering profile of a single scatterer, and taking into account the scattering direction and light propagation distances in different media. The experiments are convincingly modelled, both for the backward- and forward-scattered light. With the correct scattering profile for a single strip, the complex experimental diffraction pattern is accurately reproduced. Importantly, the comparison proved very sensitive to the single strip scattering profile used in the model. Thus, we find that our technique enables sensitive experimental verification of simulated angular scattering profiles.

Acknowledgments

The authors gratefully acknowledge financial support from the PLATOS project "Localized-surface plasmons and silicon thin-film solar cells", financed by the Villum Foundation.

References

1. H. A. Atwater and A. Polman, "Plasmonics for improved photovoltaic devices," Nat. Mater. **9**, 205–213 (2010).
2. P. Spinelli, V. E. Ferry, J. van de Groep, M. van Lare, M. A. Verschuuren, R. E. I. Schropp, H. A. Atwater, and A. Polman, "Plasmonic light trapping in thin-film Si solar cells," J. Opt. **14**, 024002 (2012).
3. K. Catchpole and A. Polman, "Plasmonic solar cells," Opt. Express **16**, 21793–21800 (2008).
4. L. Novotny and N. Van Hulst, "Antennas for light," Nat. Photonics **5**, 83 (2011).
5. T. Søndergaard, Y.-C. Tsao, P. K. Kristensen, T. G. Pedersen, and K. Pedersen, "Light trapping in guided modes of thin-film silicon-on-silver waveguides by scattering from a nanostrip," J. Opt. Soc. Am. B **31**, 2036–2044 (2014).
6. J. Jung, T. Søndergaard, T. G. Pedersen, K. Pedersen, A. N. Larsen, and B. B. Nielsen, "Dyadic Green's functions of thin films: Applications within plasmonic solar cells," Phys. Rev. B **83**, 085419 (2011).
7. W. Lukosz and R. E. Kunz, "Light emission by magnetic and electric dipoles close to a plane interface. I. total radiated power," J. Opt. Soc. Am. **67**, 1607–1615 (1977).
8. J. Mertz, "Radiative absorption, fluorescence, and scattering of a classical dipole near a lossless interface: a unified description," J. Opt. Soc. Am. B **17**, 1906–1913 (2000).
9. C. Langhammer, B. Kasemo, and I. Zorić, "Absorption and scattering of light by Pt, Pd, Ag, and Au nanodisks: Absolute cross sections and branching ratios," J. Chem. Phys. **126**, 194702 (2007).
10. D. D. Evanoff and G. Chumanov, "Size-controlled synthesis of nanoparticles. 2. measurement of extinction, scattering, and absorption cross sections," J. Phys. Chem. B **108**, 13957–13962 (2004).
11. W. Lukosz, "Light emission by magnetic and electric dipoles close to a plane dielectric interface. III. radiation patterns of dipoles with arbitrary orientation," J. Opt. Soc. Am. **69**, 1495–1503 (1979).
12. W. Lukosz and R. E. Kunz, "Light emission by magnetic and electric dipoles close to a plane dielectric interface. II. radiation patterns of perpendicular oriented dipoles," J. Opt. Soc. Am. **67**, 1615–1619 (1977).
13. A. Abass, P. Gutsche, B. Maes, C. Rockstuhl, and E. R. Martins, "Insights into directional scattering: from coupled dipoles to asymmetric dimer nanoantennas," Opt. Express **24**, 19638–19650 (2016).
14. S. R. J. Brueck, "Radiation from a dipole embedded in a dielectric slab," IEEE J. Sel. Top. Quantum Electron. **6**, 899–910 (2000).
15. C. Huang, A. Bouhelier, G. Colas des Francs, A. Bruyant, A. Guenot, E. Finot, J.-C. Weeber, and A. Dereux, "Gain, detuning, and radiation patterns of nanoparticle optical antennas," Phys. Rev. B **78**, 155407 (2008).
16. A. G. Curto, G. Volpe, T. H. Taminiau, M. P. Kreuzer, R. Quidant, and N. F. van Hulst, "Unidirectional emission of a quantum dot coupled to a nanoantenna," Science **329**, 930–933 (2010).

Received 21 Feb 2019; revised 9 Apr 2019; accepted 11 Apr 2019; published 2 May 2019

Optics EXPRESS

17. T. Coenen, E. J. R. Vesseur, A. Polman, and A. F. Koenderink, "Directional emission from plasmonic Yagi-Uda antennas probed by angle-resolved cathodoluminescence spectroscopy," Nano Lett. **11**, 3779–3784 (2011).
18. M. Schwind, V. D. Miljković, M. Zäch, V. Gusak, M. Käll, I. Zorić, and P. Johansson, "Diffraction from arrays of plasmonic nanoparticles with short-range lateral order," ACS Nano **6**, 9455–9465 (2012).
19. E. Skovsen, T. Søndergaard, J. Fiutowski, H.-G. Rubahn, and K. Pedersen, "Surface plasmon polariton generation by light scattering off aligned organic nanofibers," J. Opt. Soc. Am. B **29**, 249–256 (2012).
20. K.-H. Su, Q.-H. Wei, X. Zhang, J. J. Mock, D. R. Smith, and S. Schultz, "Interparticle coupling effects on plasmon resonances of nanogold particles," Nano Lett. **3**, 1087–1090 (2003).
21. W. Rechberger, A. Hohenau, A. Leitner, J. Krenn, B. Lamprecht, and F. Aussenegg, "Optical properties of two interacting gold nanoparticles," Opt. Commun. **220**, 137 – 141 (2003).
22. T. M. Søndergaard, *Green's Function Integral Equation Methods in Nano-Optics* (CRC Press, 2019). (Chap. 4).
23. Y. Mizokawa, O. Komoda, and S. Miyase, "Long-time air oxidation and oxide-substrate reactions on GaSb, GaAs and GaP at room temperature studied by X-ray photoelectron spectroscopy," Thin Solid Films **156**, 127 – 143 (1988).
24. L. Feng, L.-D. Zhang, H. Liu, X. Gao, Z. Miao, H.-C. Cheng, L. Wang, and S. Niu, "Characterization study of native oxides on GaAs(100) surface by XPS," Proc. SPIE **8912**, 89120N (2013).
25. W. Cai, H. Zhong, and L. Zhang, "Optical measurements of oxidation behavior of silver nanometer particle within pores of silica host," J. Appl. Phys. **83**, 1705–1710 (1998).
26. M. D. McMahon, R. Lopez, H. M. Meyer, L. C. Feldman, and R. F. Haglund, "Rapid tarnishing of silver nanoparticles in ambient laboratory air," Appl. Phys. B **80**, 915–921 (2005).
27. Optical data from Sopra SA, "GaAs optical constants," http://www.sspectra.com/sopra.html.

Received 21 Feb 2019; revised 9 Apr 2019; accepted 11 Apr 2019; published 2 May 2019